ELSEVIER

Biophysical Chemistry 107 (2004) 299–316

Biophysical Chemistry

www.elsevier.com/locate/bpc

Effects of inert volume-excluding macromolecules on protein fiber formation. II. Kinetic models for nucleated fiber growth

Damien Hall*, Allen P. Minton

Section on Physical Biochemistry, Laboratory of Biochemistry and Genetics, National Institute of Diabetes and Digestive and Kidney Diseases, National Institutes of Health, Bethesda, MD, USA

Received 27 August 2003; received in revised form 30 September 2003; accepted 30 September 2003

Abstract

A sequential model for nucleated protein fiber formation is proposed that is similar in broad outline to models proposed previously (Thermodynamics of the Polymerization of Protein, Academic Press, New York, (1975); Biophys. J. 50 (1986) 583) but generalized to allow for thermodynamic nonideality resulting from a high degree of volume occupancy by inert macromolecular cosolutes (macromolecular crowding). The effect of volume occupancy on the rate of fiber formation is studied in the transition-state rate-limited regime through systematic variation of rate-limiting step (prenuclear oligomer formation, nucleus formation or fiber growth), shape of prenuclear oligomer, size of nucleus, extent of reversibility, nature of inert cosolute (hard globular particle or random coil polymer) and size of inert cosolute relative to that of fiber-forming protein. It is found that crowding can accelerate the rate of fiber formation by as much as several orders of magnitude. The extent of acceleration for a given degree of volume occupancy depends upon several factors, the most conspicuous of which is the stoichiometry of the nucleus. In contrast, the rate of redistribution of fiber length, which occurs on a much slower time scale than polymer formation, is found to be insensitive to the extent of crowding.

Keywords: Macromolecular crowding; Thermodynamic nonideality; Rate equations

1. Introduction

The biologically widespread process of protein fiber formation has traditionally been analyzed in the context of models positing an initial thermodynamically disfavored process of nucleation followed by the thermodynamically favored process of fiber growth [1–3]. The overall process is typically studied by preparing a solution of protein under conditions such that polymerization is inhibited, and then initiating polymerization at time zero by rapidly changing solution conditions to those favoring polymerization, by for example changing temperature or pH, or adding small molecule cofactors facilitating polymerization [4–6]. A variety of kinetic models for protein fiber formation have been proposed and analyzed extensively [2,7–12], all of which apply exclusively to proteins polymerizing under conditions such that non-specific solute–solute interaction is negligible,

*Corresponding author. Chemistry Department, Cambridge University, Lensfield Road, Cambridge CB2-1NE, UK. Tel.: +44-1223-763-845; fax: +44-1223-763-849.
E-mail address: drh32@cam.ac.uk (D. Hall).

0301-4622/04/$ - see front matter © 2003 Elsevier B.V. All rights reserved.
doi:10.1016/j.bpc.2003.09.016

i.e. under thermodynamically ideal conditions. However, it has become increasingly appreciated that in physiological media, neglect of non-specific solute–solute interaction, in particular excluded volume interactions arising from steric repulsion ('macromolecular crowding'), may lead to qualitatively incorrect estimates of the rates and equilibria of macromolecular associations [13–17]. It has been shown experimentally that excluded volume in solutions of high total macromolecular content may profoundly influence the rate and extent of protein fiber formation [18–24], and models for these effects in specific systems have been proposed [18,24–26]. We have previously presented a general analysis of the effect of excluded volume on the equilibria of fiber formation [27]. The equilibrium analysis was based upon extensions of the widely accepted Oosawa–Asakura paradigm for nucleated linear self-assembly [2], to allow for non-specific steric interactions between the dilute fiber-forming protein and an inert macromolecular cosolute ('crowder') present at arbitrary concentration. The purpose of the present work is to build on the preceding equilibrium treatment and develop quantitative models for the effect of excluded volume on protein fiber formation that are more general than those presented earlier.

In the present work, we develop a kinetic model of reversible fiber nucleation and growth that is similar to, but more general[1] than, the model of Goldstein and Stryer [9] under thermodynamically ideal conditions. We then extend the model to nonideal conditions by allowing for the effect of excluded volume on the various rate constants appearing in the model. The behavior of the extended model under different rate-limiting conditions is then explored as a function of the concentration of crowder.

[1] We have tried to make our model of nucleation as general as possible by considering parameter regimes that cover behavior from kinetically limited to thermodynamically limited nucleation. By spanning this region (from one limiting behavior to another) we accommodate, in a general fashion, the gross features of all conceivable experimental nucleated polymerization behavior—thereby making our modeling strategy more wide ranging than previous efforts that are reliant upon the pre-equilibrium approximation (thermodynamically limited nucleation).

2. Theory and methods

2.1. Kinetic models for fiber formation

We posit an infinite series of reversible stepwise additions of monomer to *i*-mer:

$$A_1 + A_{i-1} \rightleftarrows A_i \tag{1}$$

with a second-order rate constant for association $k_f(i)$ and a first-order rate constant for dissociation $k_b(i)$. As in previous models of a similar nature [2,7,9] we postulate that there exists a unique oligomer size, with a stoichiometry n, such that the kinetics of addition to oligomers of size n or greater are distinct from those of addition to smaller oligomers. We shall refer to n-mer as nucleus, and assert that it represents the smallest structural unit that presents a site for the addition of subsequent monomeric subunits which is structurally and energetically equivalent to that presented by all larger oligomers. For the sake of simplicity, Goldstein and Stryer [9] postulated that $k_f(i) = k_f$ and $k_b(i) = k_b$ for all $i \leqslant n$, and that $k_f(i) = k_f^G$ and $k_b(i) = k_b^G$ for all $i > n$. We shall retain the condition that all stepwise additions to species with $i > n$ have identical rate constants, but allow the formation of oligomers with $i \leqslant n$ to have size-dependent forward and backward rate constants. In particular, we feel that the addition of monomer to $(n-1)$-mer should be kinetically distinguished from the addition reactions preceding and following it, as it represents a combination of binding of monomer to a prenuclear complex and conformational rearrangement to form the nucleus, a situation depicted schematically in Fig. 1. In addition, it will be shown subsequently that depending upon assumptions made regarding the shape of prenuclear oligomers, excluded volume may differentially affect different prenuclear stepwise addition rate constants.

The general reaction scheme indicated by Eq. (1) above then leads to the following set of rate equations:

For $i = 2$ to $n-1$:

$$\frac{dc_i}{dt} = k_f(i)c_1c_{i-1} - [k_b(i) + k_f(i+1)c_1]c_i + k_b(i+1)c_{i+1} \tag{2}$$

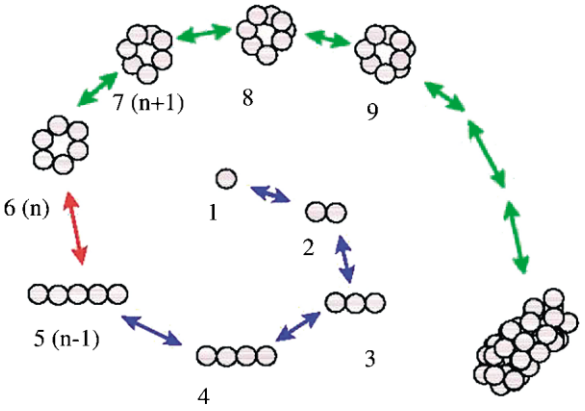

Fig. 1. Schematic depiction of the stepwise addition model for nucleated fiber formation. Blue arrows indicate addition of monomer to soluble oligomer with association rate constant $k_f(i)$ and dissociation rate constant $k_b(i)$, where i is the stoichiometry of the product. The red arrow indicates addition of monomer to $n-1$-mer, with association rate constant $k_f(n)$ and dissociation rate constant $k_b(n)$. This step is energetically distinguished from prior steps due to a coupled isomerization leading to the formation of nucleus. Green arrows indicate addition of monomer to nucleus and all larger species, with association rate constant k_f^G and dissociation rate constant k_b^G.

$$\frac{dc_n}{dt} = k_f(n)c_1c_{n-1} - [k_b(n) + k_f^G c_1]c_n + k_b^G c_{n+1} \quad (3)$$

For $i = n+1$ to ∞:

$$\frac{dc_i}{dt} = k_f^G c_1 c_{i-1} - [k_b^G + k_f^G c_1]c_i + k_b^G c_{n+1} \quad (4)$$

In principle, one can obtain the time evolution of the system by solving Eqs. (2) and (3) together with an arbitrarily large set of equations of the form of Eq. (4). This is not generally practical, but in certain special cases described below, the distribution of polymer sizes at equilibrium is sufficiently narrow to enable a full solution of this kind.

For a more general exploration of parameter space we adopt an approximate method for truncating the set of required rate equations, which is an extension of that initially suggested by Oosawa and Asakura [2] for the case of irreversible fiber growth. The total number of moles of polymer N_{poly} and the total number of moles of monomer in polymer c_{poly} are defined as follows:

$$N_{poly} \equiv \sum_{i=n+1}^{\infty} c_i \quad (5)$$

$$c_{poly} = \sum_{i=n+1}^{\infty} ic_i \quad (6)$$

We shall assume that polymer does not fracture, so that the addition of monomer to growing polymer does not change the number of moles of polymer. Hence the rate of change of N_{poly} is equal to the rate of formation of nuclei:

$$\frac{dN_{poly}}{dt} = k_f^G c_1 c_n - k_b^G c_{n+1} \quad (7)$$

Straightforward differentiation of Eq. (6) and summation of series lead to

$$\frac{dc_{poly}}{dt} = n[k_f^G c_1 c_n - k_b^G c_{n+1}] + [k_f^G c_1 - k_b^G]N_{poly} + k_f^G c_1 c_n \quad (8)$$

Finally, conservation of mass yields:

$$\frac{dc_1}{dt} = -\sum_{i=2}^{n} i\frac{dc_i}{dt} - \frac{dc_{poly}}{dt} \quad (9)$$

In order to truncate the number of rate equations that must be solved without introducing significant error into the calculated time dependence of c_{poly}, we introduce the following approximation. First, we limit the conditions of study to those in which the rate of growth of polymer by addition exceeds the rate of loss by monomer dissociation. (This approximate method is, therefore, not suitable for simulating the time dependence of net depolymerization.) It follows that there exists some number $n_{max} > n$ such that back-dissociation from species larger than n_{max} has a negligible effect upon the time-dependent concentration of nucleus. Under such conditions, we need to calculate explicitly the concentrations of only those species with

$i \leqslant n_{\max}$, and Eq. (4) is replaced by the following two rate equations:

For $i = n+1$ to $n_{\max}-1$:

$$\frac{dc_i}{dt} = k_f^G c_1 c_{i-1} - [k_b^G + k_f^G c_1] c_i + k_b^G c_{n+1} \quad (10)$$

$$\frac{dc_{n_{\max}}}{dt} = k_f^G c_1 c_{n_{\max}-1} - [k_b^G + k_f^G c_1] c_{n_{\max}} \quad (11)$$

where dissociation from species $i = n_{\max}+1$ is neglected in Eq. (11).

2.2. Scaled (dimensionless) rate equations

Let c_{tot} denote the total protein concentration in moles per liter of monomer, and k_o a reference second-order rate constant. We then define the following scaled (dimensionless) variables:

$$\chi_f(i) \equiv k_f(i)/k_o$$
$$\chi_b(i) \equiv k_b(i)/(k_o c_{tot})$$
$$\chi_f^G \equiv k_f^G/k_o$$
$$\chi_b^G \equiv k_b^G/(k_o c_{tot})$$

$f_i \equiv i c_i / c_{tot}$ (mass fraction of species i)

$f_{poly} \equiv c_{poly}/c_{tot}$ (mass fraction of protein in polymer)

$g_{poly} = N_{poly}/c_{tot}$ (mole of polymer/mole subunit)

$$t^* = k_o c_{tot} t$$

It may be seen that k_o is simply the actual value of that particular second-order rate constant whose scaled value is set equal to unity. By substitution of the scaled variables defined above into rate equations Eqs. (2)–(11), we obtain the following equivalent set of scaled rate equations:

For $i = 2$ to $n-1$:

$$\frac{df_i}{dt^*} = i\chi_f(i) f_1 f_{i-1}/(i-1) - [\chi_b(i) + \chi_f(i+1) f_1] f_i + i\chi_b(i+1) f_{i+1}/(i+1) \quad (12)$$

$$\frac{df_n}{dt^*} = n\chi_f(n) f_1 f_{n-1}/(n-1) - [\chi_b(n) + \chi_f^G f_1] f_n + n\chi_b^G f_{n+1}/(n+1) \quad (13)$$

For $i = n+1$ to $n_{\max}-1$:

$$\frac{df_i}{dt^*} = i\chi_f^G f_{i-1}/(i-1) - [\chi_b^G + \chi_f^G f_1] f_i + i\chi_b^G f_{i+1}/(i+1) \quad (14)$$

$$\frac{df_{n_{\max}}}{dt^*} = n_{\max}\chi_f^G f_{n_{\max}-1}/(n_{\max}-1) - [\chi_b^G + \chi_f^G f_1] f_{n_{\max}} \quad (15)$$

$$\frac{df_{poly}}{dt^*} = (n+1)\chi_f^G f_1 f_n/n - n\chi_b^G f_{n+1}/(n+1) + [\chi_f^G f_1 - \chi_b^G] g_{poly} \quad (16)$$

$$\frac{dg_{poly}}{dt^*} = \chi_f^G f_1 f_n/n - \chi_b^G f_{n+1}/(n+1) \quad (17)$$

$$\frac{df_1}{dt^*} = -\sum_{i=2}^{n} \frac{df_i}{dt^*} - \frac{df_{poly}}{dt^*} \quad (18)$$

The validity of the truncation procedure, wherein back dissociation from species larger than $n_{\max}$ is assumed to have a negligible effect upon the concentration of nucleus, may be verified in one of two ways. First, one may compare solutions of sets of equations with identical values of the rate constants and n, but with different values of $n_{\max}$. If there exists a value of $n_{\max}$ ($n_{\max}$*) such that the solutions are independent of the value of $n_{\max}$ for all $n_{\max} > n_{\max}$*, then the truncation procedure is validated for $n_{\max} \geqslant n_{\max}$*. (Note that truncation is automatically valid for all values of $n_{\max} > n$ if $\chi_b^G = 0$.) Alternatively, for a limited number of parameter sets, one may compare the time dependence of f_{poly} calculated using the truncated model with that calculated using the full model, i.e. Eqs. (2) and (3) with a large number of equations of the form of Eq. (4), sufficient to account for all species of polymer that are significantly populated at equilibrium. It was found, as reported below, that in contrast to the distribution of polymer lengths, the time dependence of f_{poly} is well

described by the solution of the truncated equations with a small value of n_{max}. Therefore, unless explicitly stated otherwise, calculations of $f_{poly}(t)$ alone were carried out using a default value of $n_{max}=n+3$.

The use of scaled rate equations permits us to explore the various types of kinetic behavior which may be exhibited by the model specified above without having to specify actual rate constants or concentrations, and with a reduced number of variables. A particular solution of the scaled equations may be linearly transformed to the equivalent solution of the actual rate equations upon specification of the values of k_o and c_{tot}.

2.3. Effect of excluded volume on rate constants

It is assumed that the concentration of fiber-forming protein is sufficiently dilute that non-specific excluded volume interactions between species of this protein are negligible. As in Hall and Minton [27], excluded volume effects are attributed exclusively to steric repulsion between individual species of the fiber-forming protein and between a chemically inert macromolecular crowder that may be present at arbitrary concentration.

Hall and Minton [27] adopted a hard particle model for self-assembly in which monomer was represented as a spherical particle of radius r_1, i-mers between 1 and n were represented as spherical particles of radius $i^{1/3}r_1$, and i-mers of stoichiometry $n+1$ and greater were represented as spherocylindrical particles with cylindrical radius r_n and cylindrical length/diameter ratio $2(i-n)/(3n)$. This model, referred to as the *globular prenuclear oligomer* model, is depicted schematically in Figure 1 of Hall and Minton [27]. In the present work we additionally employ an alternate hard particle model, in which i-mers between 2 and $n-1$ are assumed to be linear rather than globular, and are represented by spherocylindrical particles of cylindrical radius r_1 and cylindrical length/diameter ratio of $2(i-1)/3$. This model, referred to as the *linear prenuclear oligomer* model, is depicted schematically in Fig. 1.

In principle, the effect of excluded volume upon reaction rate depends upon whether the overall reaction rate is limited by the rate of conversion of the transition-state complex to product (reaction-limited kinetics) or whether it is limited by the rate of bimolecular encounter between reactants (diffusion-limited kinetics) [15]. However, at the present time there is no satisfactory quantitative theory for the effect of excluded volume upon diffusion-limited kinetics in a crowded medium, and the present treatment is, therefore, limited to the analysis of reaction- (or transition state-) limited kinetics. For the sake of comparison of model predictions with experiment, the solution conditions under which a particular protein fiber-forming reaction is studied may be adjusted to achieve a reaction rate sufficiently slow to ensure that the process is not diffusion rate-limited. We postulate that the transition-state complex excludes essentially the same volume to cosolute as product, leading to [15,28]

$$\chi_f(i)=\chi_f(i)^o\frac{\gamma_1\gamma_{i-1}}{\gamma_i}\equiv\chi_f(i)^o\Gamma_i \tag{19}$$

$$\chi_b(i)=\chi_b(i)^o \tag{20}$$

where γ_i denotes the thermodynamic activity coefficient of species i, which is dependent upon the concentration of inert macromolecular additive in a manner that may be estimated from excluded volume theory [29–33], and a superscript 'o' denotes the ideal value of the superscripted variable (i.e. in the absence of excluded volume effect). For oligomers larger than nucleus, the magnitude of the nonideal effect is independent of oligomer size [27], so

$$\chi_f^G=\chi_f^{G^o}\Gamma^G \tag{21}$$

$$\chi_b^G=\chi_b^{G^o} \tag{22}$$

Unless specified otherwise, activity coefficients are calculated as a function of fractional volume occupancy ϕ using the scaled particle theory of Cotter [33] for a hard spherical crowding species with radius r_C, or using the available volume theory of Ogston [29,32] and Giddings et al. [31] for a random coil polymer crowding species, represented as a random array of hard rods with

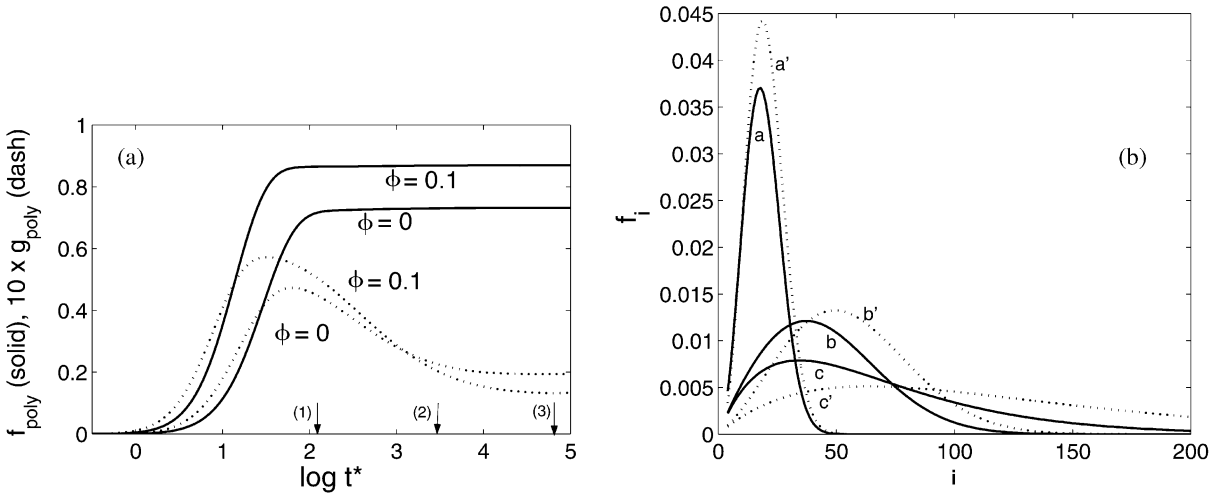

Fig. 2. Illustration of the two phases of approach to equilibrium. Simulations were carried out for $n=3$, $\chi_f^o(2\text{–}3)=0.05$, $\chi_b^o(2\text{–}3)=0.25$, $\chi_b^{G^o}=1$ and $\chi_f^{G^o}=0.25$. (A) *Solid curves:* f_{poly}, the mass fraction of protein present as polymer, as a function of log t^*. *Dashed curves:* g_{poly}, the scaled number of polymers, as a function of log t^*, multiplied by a factor of 10 for visibility. Curves were calculated for $\phi=0$ and 0.1 as indicated. The numbered arrows indicate times at which the length distributions plotted in panel B were calculated. (B) Mass fraction of i-mer plotted as a function of i for three elapsed times. Solid curves were calculated for $\phi=0$ and dashed curves for $\phi=0.1$. Curves labeled a and a′ were calculated for log $t^*=2.04$ [time point (1) in panel A], curves labeled b and b′ were calculated for log $t^*=3.43$ [time point (2) in panel A], and curves labeled c and c′ were calculated for log $t^*=4.8$ [time point (3) in panel A].

cylindrical radius r_C. Quantitative expressions for the activity coefficients are given in Hall and Minton [27].

2.4. Solution of rate equations

Rate equations were solved using one of two techniques: numerical solution of the complete set of rate equations Eqs. (2)–(4) was achieved using a fourth-order Runge-Kutta numerical integration routine [34]. The maximum allowable error was controlled by dynamically adjusting each time step so that the step would not produce a fractional change in free monomer concentration, total monomer present as polymer, concentration of nuclei, or number concentration of polymer, in excess of preselected values. The accuracy of the solutions was tested against equilibrium predictions [27] and by comparing the results of calculations made using different values of the fractional change criteria.

Solutions of the truncated scaled rate equations Eqs. (12)–(18) were obtained using the differential equation solver ODE15s in MATLAB (Mathworks, Natick, MA), implementing a variable-order Gear algorithm [35] suitable for the solution of stiff sets of ordinary differential equations. Simulations were carried out under the following default conditions unless otherwise specified: (1) initial conditions: $f_1(0)=1$, $f_i(0)=0$ for $i=2$ to n_{max}, $N_{poly}(0)=f_{poly}(0)=0$. (2) Spherical crowder model: $r_c=r_1$. (3) Linear prenuclear oligomer model. (4) All reactions were considered to be transition-state rate-limited. (5) All $k_f^o(i)$ equal for $i=2$ to $n-1$, and all $k_b^o(i)$ equal for $i=2$ to $n-1$.

3. Results

Numerical solution of the full set of rate equations Eqs. (2)–(4) in the absence of crowder yields the time course for formation of polymer (Fig. 2a) and for the evolution of the distribution of polymer lengths (Fig. 2b). It is evident that the equilibrium amount of total polymer may be attained far in advance of the equilibrium length

distribution. True equilibrium represents attainment of minimum free energy of the system. When the total amount of polymer has been formed, the enthalpy of the system has achieved a near-minimal value. The driving force for redistribution of polymer lengths is further minimization of the total free energy through maximization of the entropy of the system. Due to limitations imposed upon the kinetics of this process by model assumptions (see concluding discussion), redistribution takes place on a much slower time scale than initial polymer formation. Oosawa and co-workers [1,2,36] recognized the existence of the two distinct time scales, and suggested the following nomenclature to describe the generalized polymerization reaction coordinate.

$$\text{Monomer} \leftrightharpoons (\text{Polymer})_{\text{mass}} \leftrightharpoons (\text{Polymer})_{\text{distribution}}$$

Although the distinction is not as quite as clear-cut as suggested by the above scheme, since redistribution of polymer length is occurring concurrent with polymer growth, it represents a good starting point for the discussion of the two polymerization processes and the effect of crowding upon their respective time-dependence.

3.1. Effect of crowding on the kinetics of polymer formation

We have taken advantage of the rapidity associated with solving the truncated set of rate equations Eqs. (12)–(18) as compared to solving the full set of rate equations Eqs. (2)–(4) to provide information about the time evolution of polymer mass (f_{poly}). Even though the truncated model is simplified, it contains many variable parameters. We have attempted to explore the effect of variation in individual parameters. For obvious reasons it is not practical to explore the effect of covariation of pairs of variables, even though such effects may be significant.

The following quantities will be used to describe various features of the results. Let y denote the value of f_{poly} normalized to its asymptotic value in the long-time limit, i.e. $f_{\text{poly}}/f_{\text{poly}}^{\text{equil}}$. t_{50} is defined to be that value of t^* at which $y=0.5$. α is a kinetic cooperativity parameter, defined as

$$\alpha \equiv -\frac{\left[\dfrac{\mathrm{d}\ln(1-y)}{\mathrm{d}\ln t^*}\right]_{t^*=t_{50}}}{\ln 2} \tag{26}$$

α is equal to 1 for a function y whose rate of change with respect to t, evaluated at t_{50}, is equal to that of a single decaying exponential.[2] A value of $\alpha<1$ reflects a smaller rate of change of y with respect to t^* at $y=0.5$, which is indicative of either heterogeneous binding kinetics or negative kinetic cooperativity (apparent rate constant decreasing with y), and a value of $\alpha>1$ reflects a larger rate of change of y with respect to t^* at $y=0.5$, which is indicative of positive kinetic cooperativity (apparent rate constant increasing with y).

Results are presented graphically in one or more of the following formats.

(1) f_{poly} plotted against $\log t^*$. Plotting against $\log t^*$ rather than t^* enables both rapid and slow processes to be clearly distinguished on the same axes. If, in addition, the time course of two reactions being compared differs only in overall rate rather than mechanism, the plotted dependence of f_{poly} against $\log t^*$ will have the same shape, and differ only by a horizontal shift along the $\log t^*$ axis.

(2) $\log f_i$ $(i=1-n)$ and $\log f_{\text{poly}}$ plotted against $\log t^*$. Such a plot enables the viewer to observe the evolution of dilute species at short times as well as more concentrated species appearing at longer times.

(3) $\mathrm{d}y/\mathrm{d}t^*$ plotted against y. If the time dependence of y resembles the decaying exponential presented in [1] (with $\alpha=1$), the plot of $\mathrm{d}y/\mathrm{d}t^*$ against y will be a straight line with a constant slope of $-1/t_{\text{o}}$. A plot that is concave downward reflects kinetic heterogeneity or negatively cooperative assembly ($\alpha<1$), in which the value of the effective rate 'constant' for assembly, k_{app},

[2] α as used here is a generalization of the parameter employed in the empirical stretched exponential function $y=1-\exp[(-t/t_{\text{o}})^{\alpha}]$ commonly employed to describe time-dependent processes exhibiting kinetic cooperativity. The dependence of f_{poly} on t calculated according to the present model studied in the present work does not necessarily resemble a stretched exponential, but the value of α evaluated at $y=0.5$ has the same qualitative significance with respect to characterizing the overall time course of the reaction.

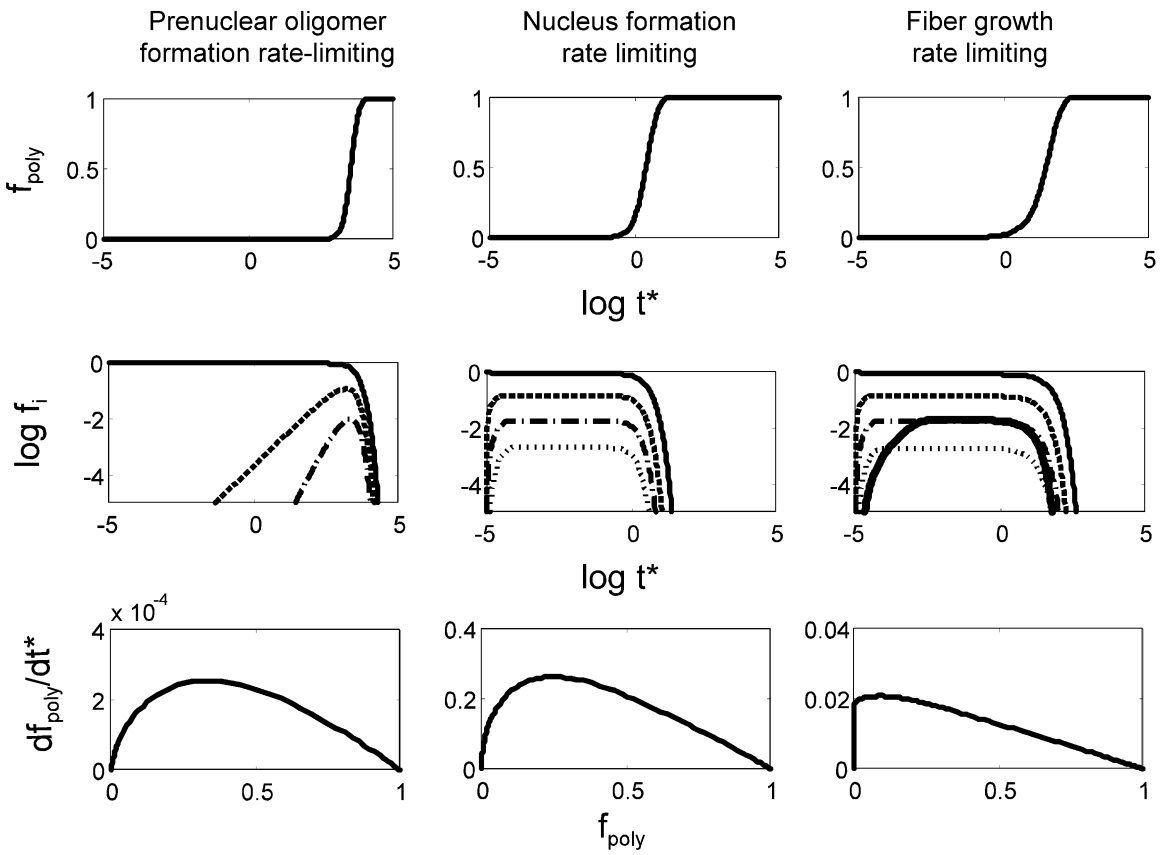

Fig. 3. Illustration of three rate-limiting regimes of the model. Simulations carried out for $n=5$, $\phi=0$. Column 1 corresponds to the prenuclear oligomer rate-limiting regime [$\chi_f^o(2\text{–}4)=10^{-4}$, $\chi_b^o(2\text{–}4)=10^{-3}$, $\chi_f^o(n)=1$, $\chi_b^o(n)=0.1$, $\chi_f^{G^o}=1$, $\chi_b^{G^o}=0$], column 2 the nucleus formation rate-limiting regime [$\chi_f^o(2\text{–}4)=10^4$, $\chi_b^o(2\text{–}4)=10^5$, $\chi_f^o(n)=1$, $\chi_b^o(n)=0.1$, $\chi_f^{G^o}=10^3$, $\chi_b^{G^o}=0$] and column 3 the fiber growth rate-limiting regime [$\chi_f^o(2\text{–}4)=10^4$, $\chi_b^o(2\text{–}4)=10^5$, $\chi_f^o(n)=10^4$, $\chi_b^o(n)=10^3$, $\chi_f^{G^o}=1$, $\chi_b^{G^o}=0$]. *Row 1:* plots of f_{poly} as a function of $\log t^*$. *Row 2:* plots of $\log f_i$ for $i=1$ to n as a function of $\log t^*$ (solid line—$\log f_1$, long dashed line—$\log f_2$, dot-dashed line—$\log f_3$, dotted line—$\log f_4$, thick solid line—$\log f_5$). The absence of a line corresponding to a given species j indicates that the maximum calculated abundance of $\log f_j$ was less than -5. *Row 3:* plots of df_{poly}/dt^* against f_{poly}.

decreases with increasing extent of assembly. Conversely, a plot that is concave upward reflects positively cooperative assembly ($\alpha>1$), in which the value of k_{app} initially increases with increasing extent of assembly.

3.1.1. Ideal kinetics in different rate-limiting regimes

Rate equations Eqs. (12)–(18) were solved for three sets of parameter values in the ideal limit (fractional volume occupancy $\phi=0$), given in the caption to Fig. 3. In parameter set *a*, the dimensionless rate constant for the addition of monomer to prenuclear oligomer is set to a value much smaller than those for the formation of nucleus or for polymer growth, generating a situation in which the formation of prenuclear oligomers is slow, followed by rapid conversion of $n-1$-mer to n-mer and thence to polymer. In parameter set *b*, the dimensionless rate constant for the addition of monomer to $n-1$-mer (i.e. for nucleus formation) is set to a value much smaller than those for the addition of monomer to smaller prenuclear oligomers or for polymer growth, generating a situation in which prenuclear oligomers are formed almost instantaneously, attaining an equilibrium in

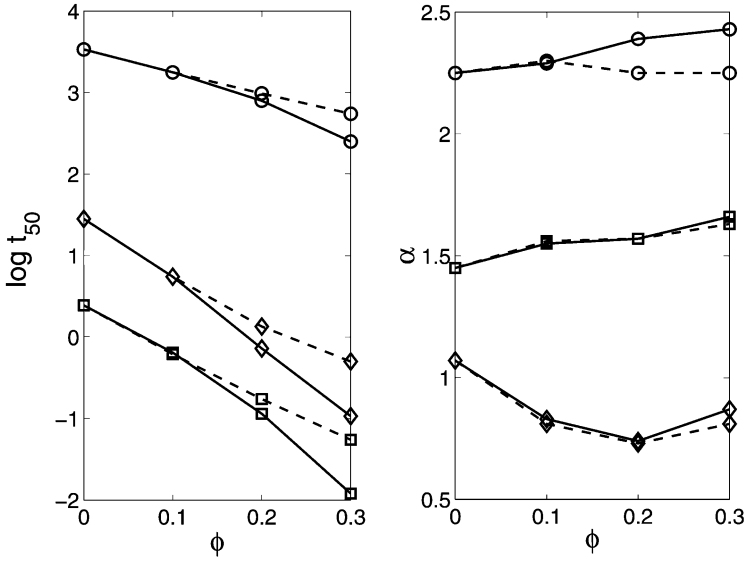

Fig. 4. Dependence of $\log t_{50}$ and α on ϕ, calculated using the model for spherical crowder ($r_C = r_1$, solid lines) and random coil polymeric crowder ($r_C = 0.5r_1$, dashed lines) in the prenuclear oligomer rate-limiting regime [$\chi_f^o(2\text{–}4) = 10^{-3}$, $\chi_b^o(2\text{–}4) = 10^{-2}$, $\chi_f^o(n) = 1$, $\chi_b^o(n) = 0.1$, $\chi_f^{G^o} = 1$, $\chi_b^{G^o} = 0$] (circles), the nucleus formation rate-limiting regime [$\chi_f^o(2\text{–}4) = 10^4$, $\chi_b^o(2\text{–}4) = 10^5$, $\chi_f^o(n) = 1$, $\chi_b^o(n) = 0.1$, $\chi_f^{G^o} = 10^3$, $\chi_b^{G^o} = 0$] (squares), and the fiber growth rate-limiting regime [$\chi_f^o(2\text{–}4) = 10^4$, $\chi_b^o(2\text{–}4) = 10^5$, $\chi_f^o(n) = 10^4$, $\chi_b^o(n) = 10^3$, $\chi_f^{G^o} = 1$, $\chi_b^{G^o} = 0$] (diamonds).

solution that lasts for several orders of magnitude in time due to the kinetic bottleneck arising from the slow conversion of $n-1$-mer to n-mer. The material that is converted to n-mer (nucleus) is then rapidly converted to polymer, and hence does not accumulate. In parameter set *c*, dimensionless rate constants for the addition of monomer to all prenuclear oligomers, including $n-1$-mer, are set to values much higher than that for the growth of polymer, generating a situation in which oligomers up to and including n-mer are rapidly formed, and nucleus accumulates due to the slow conversion of n-mer to $n+1$-mer and higher polymers. This last (polymer growth rate-limited) situation is analogous to the introduction of seeds into a supersaturated solution of protein, and the resulting kinetics are similar, namely, the non-cooperative (slow) addition of monomer to the rapidly formed nuclei and subsequently formed polymers.

It is emphasized that even though parameters may be selected so that the ideal behavior of the model falls clearly within one of the rate-limiting regimes delineated above, more complex kinetics may be observed in a crowded medium. Differential excluded volume effects on the three sets of rate constants (prenuclear addition, nuclear addition/isomerization, and growth) can lead to hybrid behaviors in systems that exhibit only one in the absence of crowding.

3.1.2. Influence of choice of rate-limiting step and crowder type

Rate equations Eqs. (12)–(18) were solved for three sets of ideal rate parameters given in the caption to Fig. 3, corresponding to the three rate-limiting regimes delineated in the preceding section in the limits of reversible and irreversible growth, and two sets of excluded volume parameters given in the caption to Fig. 4, corresponding to excluded volume theories appropriate for a spherical crowder [30,33,37] or a random coil polymeric crowder [29,31,32]. The results are summarized as plots of $\log t_{50}$ and α as functions of ϕ in Fig. 4. It is observed that for all the three rate-limiting regimes, $\mathrm{d}\log t_{50}/\mathrm{d}\phi$ is approximately independent of ϕ for the random coil polymer

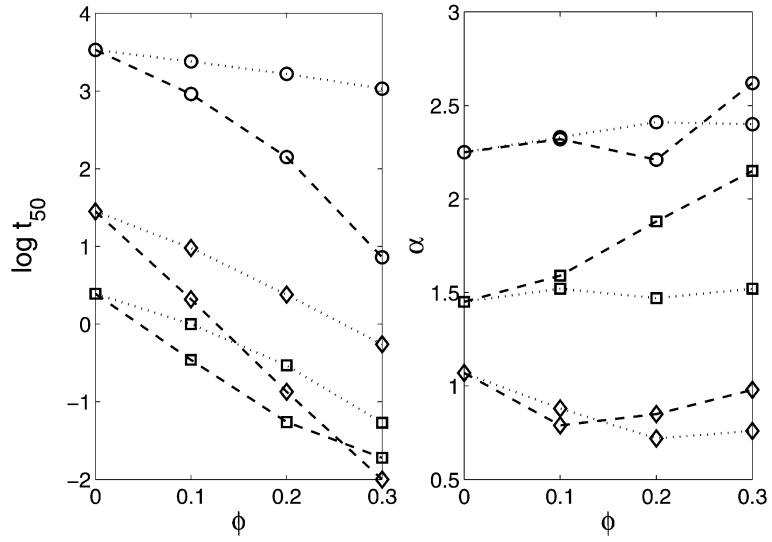

Fig. 5. Dependence of log t_{50} and α on ϕ, calculated using the model for spherical crowder wth $r_C = 3^{1/3} r_1$ (dotted lines) and $r_C = r_1/3^{1/3}$ (dashed lines) in the prenuclear oligomer rate-limiting regime [$\chi_f^o(2\text{–}4) = 10^{-4}$, $\chi_b^o(2\text{–}4) = 10^{-3}$, $\chi_f^o(n) = 1$, $\chi_b^o(n) = 0.1$, $\chi_f^{G^o} = 1$, $\chi_b^{G^o} = 0$] (circles), the nucleus formation rate-limiting regime [$\chi_f^o(2\text{–}4) = 10^4$, $\chi_b^o(2\text{–}4) = 10^5$, $\chi_f^o(n) = 1$, $\chi_b^o(n) = 0.1$, $\chi_f^{G^o} = 10^3$, $\chi_b^{G^o} = 0$] (squares), and the fiber growth rate-limiting regime [$\chi_f^o(2\text{–}4) = 10^4$, $\chi_b^o(2\text{–}4) = 10^5$, $\chi_f^o(n) = 10^4$, $\chi_b^o(n) = 10^3$, $\chi_f^{G^o} = 1$, $\chi_b^{G^o} = 0$] (diamonds).

model, whereas the absolute value of $d \log t_{50}/d\phi$ increases with increasing ϕ for the spherical crowder model. This seems to be a general consequence of the difference between the two theories used to calculate activity coefficients. According to the Ogston/Giddings available volume theory used to calculate activity coefficients in a random-coil polymer crowder [29,31,32], $d \ln \gamma/d\phi$ is independent of ϕ, whereas in the Cotter scaled particle theory used to calculate activity coefficients in a spherical crowder [33], $d \ln \gamma/d\phi$ increases significantly with increasing ϕ. While the kinetic cooperativity associated with fiber formation, as reflected in the value of α, is different for the three rate-limiting regimes, that of a given rate-limiting regime does not seem to be greatly affected by changes in volume occupancy as calculated by either theory. For each rate-limiting regime, variation of the ideal forward and backward rate constants of the rate-limiting step was found to have an effect only on log t_{50}^o, and minimal or negligible effect on both $d \log t_{50}/d\phi$ and α (data not shown).

3.1.3. Influence of reversibility

The simulations described above, for all three rate-limiting regimes, were repeated, setting $\chi_b^G = 0.25$ rather than 0, so that the equilibrium value of f_{poly} is reduced from 1.0 to 0.75. It was found in all cases that the calculated dependence of log t_{50} on ϕ was almost exactly the same as in the irreversible case. The absolute values of α were altered by at most 0.1. It thus appears that the kinetics of polymer formation and the influence of crowding on those kinetics—in contrast to the ultimate amount of polymer formed at equilibrium—are essentially identical to the effects calculated for irreversible systems. We thus conclude that the general effects of crowding on the kinetics of fiber formation are insensitive to variation in the equilibrium solubility of polymer.

3.1.4. Influence of crowder size

Rate equations Eqs. (12)–(18) were solved for parameter sets characteristic of the three different rate-limiting regimes, with excluded volume effects calculated for a spherical crowder with

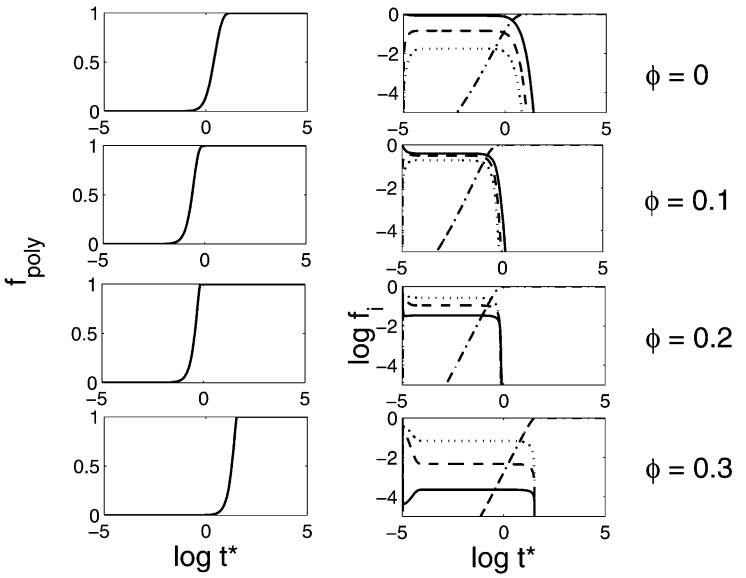

Fig. 6. Dependence of f_{poly} and $\log f_i$ on $\log t^*$, calculated for $r_C = r_1/2$ in the nucleus formation rate-limiting regime [$\chi_f^o(2\text{–}4) = 10^4$, $\chi_b^o(2\text{–}4) = 10^5$, $\chi_f^o(n) = 1$, $\chi_b^o(n) = 0.1$, $\chi_f^{G^o} = 10^3$, $\chi_b^{G^o} = 0$] at different values of ϕ. In column 2, $\log f_1$ is plotted as a solid line, $\log f_2$ as a dashed line, $\log f_3$ as a dotted line and $\log f_{poly}$ as a dot-dashed line.

mass 1/3, 1 and 3 times that of the monomer of fiber-forming protein (i.e. hard sphere radius $(1/3)^{1/3}$, 1 and $3^{1/3}$ that of the monomer). The results are summarized in Fig. 4 (solid lines) and Fig. 5. For a given volume or mass fraction of spherical crowder, the accelerating effect of crowding is more pronounced for a smaller crowder than that for a larger crowder. This is because at a fixed weight/volume concentration of crowder, there will be a higher number density (or molar concentration) of the smaller species of crowder molecules, resulting in a larger effect upon the activity coefficients of the fiber-forming species [15].[3]

An apparently anomalous result was obtained when a very small crowding agent ($r_C = 0.5r_1$) was specified. Under these conditions, t_{50} initially decreases strongly with increasing ϕ, reaches a minimum, and then begins to increase as ϕ increases further. This behavior occurs when crowding enhances the tendency of protein to self-associate to such an extent that monomer becomes substantially depleted, suppressing the rate of growth of the polymer. An example of this behavior is presented in Fig. 6.

3.1.5. Influence of oligomer shape assumption

Rate equations Eqs. (12)–(18) were solved for both the globular and linear prenuclear oligomer models for a variety of rate constant sets in all three rate-limiting regimes. In all cases, the values of $\log t_{50}$ calculated for a given set of rate constants and a given value of ϕ using the two oligomer models differed by no more than approximately 0.2, and the values of α differed by no more than approximately 0.1, indicating that variation in the assumed geometry of prenuclear oligomers does not have a major effect on the kinetic consequences of crowding.

3.1.6. Influence of nucleus size

Rate equations Eqs. (12)–(18) were solved for parameter sets characteristic of each of the three rate-limiting regimes, with $n = 2$, 5 and 10, with

[3] This relationship does not hold for random coil polymeric crowders for reasons discussed elsewhere [15]. It should also be noted that the predicted increase in activity with decreasing spherical crowder size is expected to hold only in the regime where both crowder and tracer are macromolecules, i.e. so large that the quantal nature of solvent may be safely neglected [38].

$n_{max} = n + 3$. The results are summarized in Fig. 7. To facilitate comparison between results obtained from different values of n, plots of $\Delta \log t_{50}$ ($= \log t_{50}/t_{50}^{o}$) as a function of ϕ are presented in lieu of plots of $\log t_{50}$ as a function of ϕ. It is evident that the accelerating effect of crowding is much greater for reactions that are rate limited by the formation of nuclei or fiber growth than that by the rate of prenuclear oligomer formation. The effect of nucleus size does not in general affect the apparent kinetic cooperativity of the reaction, except for the case of $n = 10$ in the prenuclear oligomer formation rate-limited reaction.

3.1.7. Effect of crowding on the kinetics of polymer length redistribution

The results presented in the preceding section indicated only relatively minor quantitative differences in the effects of different crowding agents and different pre-nuclear geometries on the kinetics of polymer production. Since the solution of the full set of rate equations is much more computation-intensive than the solution of the truncated set, our exploration of long-time behavior is limited to the effects of spherical crowding agent on the spherical prenuclear oligomer model. We define the *initial length distribution* to be that particular distribution of polymer lengths attained when the total polymer concentration first reaches its final (quasi-equilibrium) value, and the *final length distribution* to be the distribution attained in the limit of long time, i.e. at true equilibrium. It is emphasized that crowding may affect the kinetics of polymer length redistribution process by (i) altering both the initial and final distributions of polymer length and by (ii) possibly altering the rates of individual redistribution reactions.

3.1.8. Influence of rate-limiting step and crowding levels on initial length distribution

The evolution of the initial length distribution may be observed most easily by setting $\chi_b^{Go} = 0$, thereby eliminating length redistribution. The results shown in Fig. 8 indicate that depending upon the particular set of rate constants, crowding may either shorten and narrow (panel A) or lengthen and broaden (panel B) the initial length distribution. Crowding-induced broadening of the initial length distribution is less common than crowding-induced narrowing, and occurs only when prenuclear oligomers are formed so rapidly that free monomer is substantially depleted, as depicted in Fig. 6.

3.1.9. Effect of crowding on the relaxation phenomenon

In contrast to the results just presented, Hall and Minton [27] found that macromolecular crowding generally broadens and lengthens the equilibrium distribution of fiber lengths. It follows that the *amount* of relaxation that the initial distribution must undergo to reach equilibrium, expressed in terms of the number of moles of monomer that are transferred between different polymers, may be significantly altered by inclusion of crowding agents. However, the *amount* of relaxation should be distinguished from the *rate* of relaxation, the former referring to the absolute distance on the reaction coordinate, the latter being a measure of the reaction velocity in going from some intermediate distribution to the final equilibrium distribution.

This point is best demonstrated by comparing the relaxation process for a reversibly polymerizing system at different values of the fractional volume occupancy ϕ. The first example shown in Fig. 9, calculated using the parameter values given in the figure caption, represents behavior typical of a large class of prenuclear oligomer formation rate-limited sets of parameter values. A second example, shown in Fig. 10, calculated using the parameter values in the figure caption, represents behavior typical of a large class of polymer growth rate-limited sets of parameter values. We observe in both figures that following initiation of the polymerization reaction, the number of polymer molecules (proportional to g_{poly}) increases roughly in parallel with the amount of protein as polymer (f_{poly}) until the amount of polymerized protein approaches, but does not quite attain, its final value. Then g_{poly} begins to decrease, indicating a very slow relaxation of the distribution of polymer lengths to a larger mean value (compare Fig. 2)

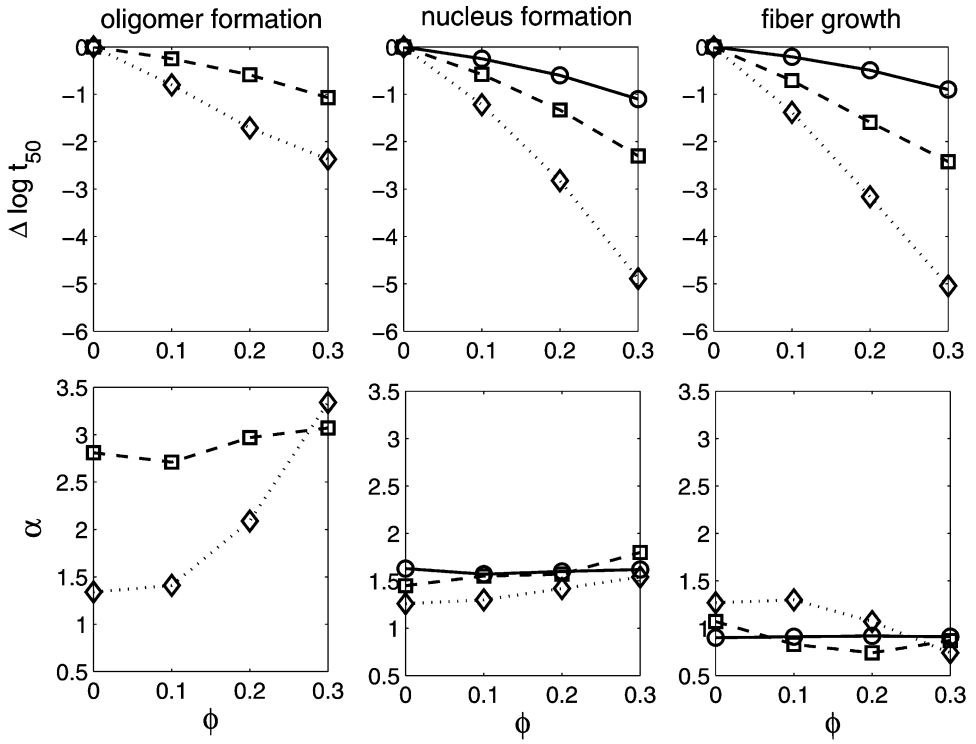

Fig. 7. Dependence of $\Delta \log t_{50}$ and α on ϕ, calculated for $n=2$ (circles), 5 (squares) and 10 (diamonds), in the prenuclear oligomer rate-limiting regime [$\chi_f^o(2 \text{ to } n-1)=1$, $\chi_b^o(2 \text{ to } n-1)=10$, $\chi_f^o(n)=10^4$, $\chi_b^o(n)=10^3$, $\chi_f^{G^o}=10^4$, $\chi_b^{G^o}=0$] (column 1), the nucleus formation rate-limiting regime [$\chi_f^o(2 \text{ to } n-1)=10^4$, $\chi_b^o(2 \text{ to } n-1)=10^5$, $\chi_f^o(n)=1$, $\chi_b^o(n)=0.1$, $\chi_f^{G^o}=10^4$, $\chi_b^{G^o}=0$] (column 2) and the fiber growth rate-limiting regime [$\chi_f^o(2 \text{ to } n-1)=10^4$, $\chi_b^o(2 \text{ to } n-1)=10^5$, $\chi_f^o(n)=10^4$, $\chi_b^o(n)=10^3$, $\chi_f^{G^o}=1$, $\chi_b^{G^o}=0$] (column 3). Note that for the special case of $n=2$, the values of $\chi_f^o(2 \text{ to } n-1)$ and $\chi_b^o(2 \text{ to } n-1)$ are not specified and the prenuclear oligomer rate-limiting regime is not defined.

that takes place at essentially constant total weight concentration of polymer.

The time dependence of g_{poly} in each of these examples may be described compactly through the use of an empirical function consisting of the sum of two stretched exponentials:

$$g_{\text{poly}}(t^*)=a_0+(a_2-a_1)\left\{1-\exp\left[-\left(\frac{t^*}{t_1}\right)^{\alpha_1}\right]\right\} +(a_3-a_2)\left\{1-\exp\left[-\left(\frac{t^*}{t_2}\right)^{\alpha_2}\right]\right\} \qquad (27)$$

in which the parameters a_i define the magnitude of the exponentials, α_i are indices of cooperativity (see preceding section) and the t_i indicate characteristic decay times. Eq. (27) was fitted by nonlinear least squares to each of the solid curves shown in Fig. 9b and Fig. 10b, and the best-fit of Eq. (27) to each curve is plotted as a dashed curve together with the original (solid) curve in the respective figures. The dependence of $\log t_i$ and α_i upon ϕ is plotted in Figs. 11 and 12. The values of $\log t_{50}$ and α characterizing the time dependence of f_{poly}, calculated as described in the previous section, are also plotted for comparison.

We may conclude from inspection of these figures that whereas the rate of polymer formation may be substantially accelerated by crowding (up to a 100-fold in the examples shown) the rate of relaxation of the length distribution (and the kinetic cooperativity of both processes) is little affected by excluded volume.

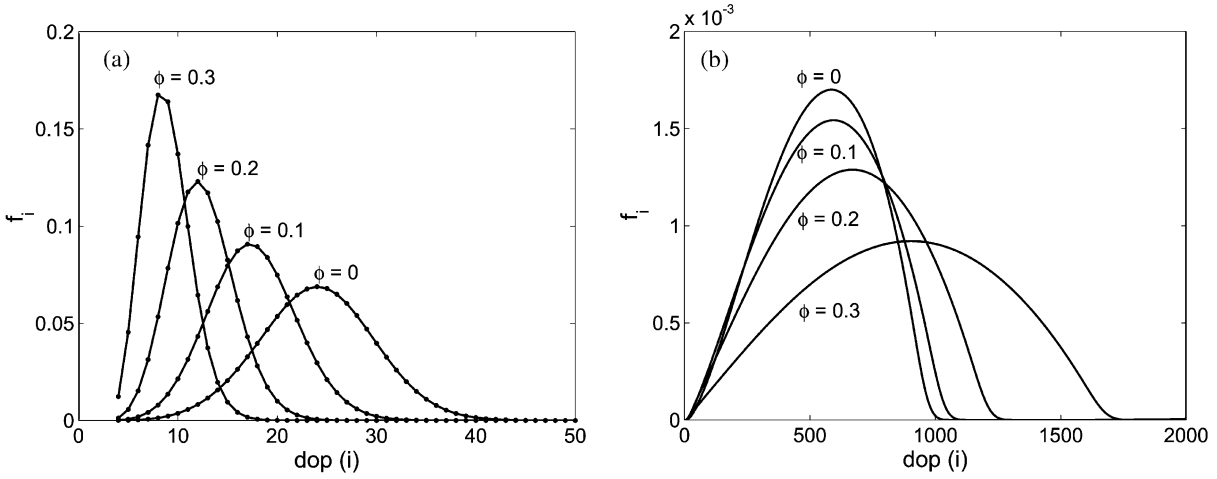

Fig. 8. Distribution of polymer length produced in the absence of polymer length distribution, calculated for $n=3$ and the following sets of rate constants: (A) $\chi_f^o(2\text{–}3)=100$, $\chi_b^o(2\text{–}3)=1000$, $\chi_f^{G^o}=1$, $\chi_b^{G^o}=0$. (B) $\chi_f^o(2\text{–}3)=0.0001$, $\chi_b^o(2\text{–}3)=0.001$, $\chi_f^{G^o}=1$, and $\chi_b^{G^o}=0$, at various degrees of fractional volume occupancy indicated in the figures. Plotted curves connect discrete values calculated for integral values of the degree of polymerization (dop), plotted as dots in panel A. These dots are not plotted in panel B due to high density.

4. Discussion

It is important to emphasize at the outset that the models formulated and studied in the present work are highly simplified and idealized representations of any process leading to the assembly of a real protein fiber. Thus, small effects are likely to represent artifacts arising from oversimplification rather than physically meaningful phenomena. However, we believe that, with two exceptions noted below, all major physical factors that can influence the formation of fibrous aggregates in a crowded medium have been at least heuristically taken into account. Hence, large qualitative (order-of-magnitude) effects observed in the simulations reported here are likely to be physically meaningful. In particular, the following observations are believed to be significant.

1. The overall rate of fiber formation may be accelerated by as much as several orders of magnitude relative to that in uncrowded solvent, depending upon the level of fractional volume occupancy by crowder and the relative size of crowding and fiber-forming species.
2. The degree of acceleration provided by a particular crowding agent depends strongly upon the size of the nucleus.
3. Compact globular crowding agents (such as globular proteins) are predicted to have a significantly greater accelerating effect on fiber formation than an equal weight/volume concentration of random-coil polymeric crowding agent of comparable molar mass and charge.
4. The kinetic cooperativity of a particular assembly process is not expected to be strongly influenced by crowding.
5. The accelerating effect of crowding on fiber formation is expected to reach a maximum at some intermediate value of fractional volume occupancy ϕ. Further increases in ϕ may lead to little change in overall fiber formation rate, or even a decrease in overall fiber formation rate, depending upon details of the mechanism.

In Fig. 7 results are presented indicating that the rate of fiber formation is strongly accelerated with increasing nucleus size, even when the overall velocity of the reaction is limited by the rate of fiber growth. At first glance one would not expect this to be the case, since the growth rate constants are independent of nucleus size. However, the

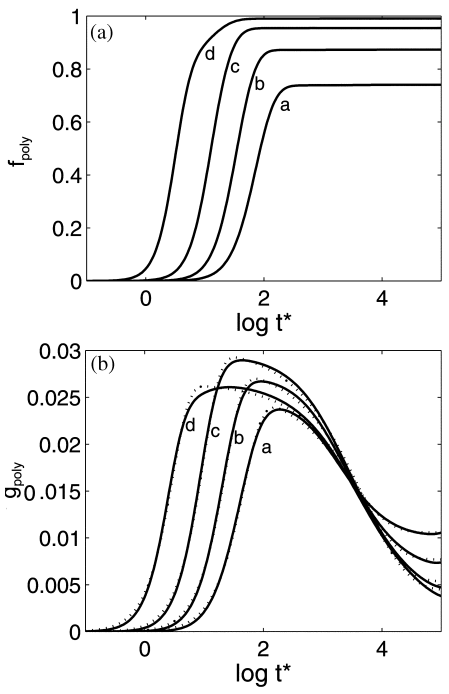

Fig. 9. Dependence of (A) f_{poly} and (B) g_{poly} on log t^*, calculated for $n=3$, $\chi_f^o(2-3)=0.01$, $\chi_b^o(2-3)=0.1$, $\chi_f^{Go}=1$, $\chi_b^{Go}=0.25$, and $\phi=0$, 0.1, 0.2 and 0.3 (curves labeled a–d, respectively). The dashed curves in panel B are the best fits of Eq. (27) to the corresponding solid curves.

growth rate depends on the steady-state molar concentration of polymer N_{poly} (or the scaled equivalent g_{poly}) as well as the rate constant for growth [Eq. (16)], and this quantity in turn depends upon the concentration of nuclei [Eq. (17)], which increases strongly with nuclear size in a crowded medium. Fiber growth is thus accelerated due to the presence of a larger number of shorter fibers, presenting more ends as sites for growth.

Solution of the full model described by rate equations Eqs. (2)–(4) reveals a very slow redistribution of fiber lengths taking place over a period of time many orders of magnitude greater than that required to attain a near-equilibrium level of total polymerization, as previously noted by Oosawa and Asakura [2]. Crowding influences this process primarily by altering the extent of redistribution rather than the rate of redistribution. The lack of a substantial effect of crowding upon the rate of length redistribution may be rationalized as follows.

Consider the transfer of monomer from a fiber initially containing j subunits to one initially containing k subunits. At a near-constant concentration of monomer, the process of transfer may be described approximately by the following reaction scheme.

$$j\text{-mer}+k\text{-mer}\underset{k_f^G}{\overset{k_b^G}{\rightleftarrows}}(j-1)\text{-mer}+\text{monomer}+k\text{-mer}$$

$$\underset{k_b^G}{\overset{k_f^G}{\rightleftarrows}}(j-1)+(k+1)\text{-mer}$$

In this approximation, the overall transfer process is symmetrical, requiring no net uptake or release of monomer, and hence no net change in excluded volume. The rate-limiting step in either direction

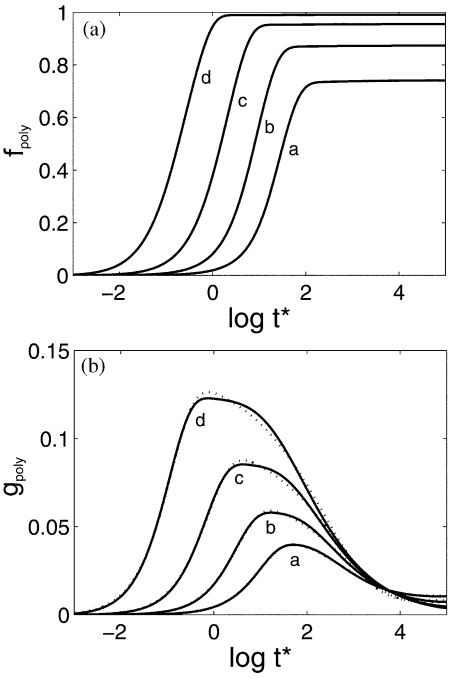

Fig. 10. Dependence of (A) f_{poly} and (B) g_{poly} on log t^*, calculated for $n=3$, $\chi_f^o(2-3)=100$, $\chi_b^o(2-3)=1000$, $\chi_f^{Go}=1$, $\chi_b^{Go}=0.25$ and $\phi=0$, 0.1, 0.2 and 0.3 (curves labeled a–d, respectively). The dashed curves in panel B are the best fits of Eq. (27) to the corresponding solid curves.

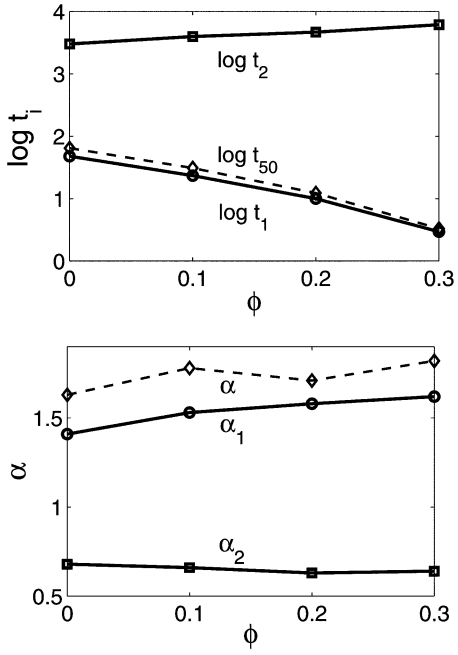

Fig. 11. ϕ-Dependence of best-fit values of $\log t_1$, $\log t_2$, α_1 and α_2 obtained from fitting Eq. (27) to $g_{poly}(t^*)$ (Fig. 9B), and ϕ-dependence of $\log t_{50}$ and α calculated for f_{poly} (t^*) (Fig. 9A).

is expected to be the dissociation of monomer from the end of a polymer, which is expected to be little affected by crowding, as described in Eqs. (19) and (20). Thus, although crowding is found to affect the initial and equilibrium polymer distributions, and hence the *extent* of redistribution, it is not expected to substantially influence the *rate* of length redistribution.

The present analysis of the kinetics of fiber formation may be distinguished from previous model studies [1,2,7,9,11,25,26,36,39,40] on two accounts. (1) Earlier treatments taking into account the effect of thermodynamic nonideality on fiber growth kinetics [25,26] were limited to specific models and did not explore the broader ramifications of crowding on fiber formation. (2) To our knowledge the present work represents the first quantitative analysis of the kinetics of fiber length redistribution. One may reasonably ask, why study redistribution, since most experimentalists are only interested in the time dependence of total polymer formation? We suggest that the length redistribution may substantially affect measured physical properties that are conventionally assumed to be a function only of the total amount of polymer, for example, the turbidity and sedimentability of the protein, and hence should be considered in interpreting the time dependence of these properties (see e.g. Refs. [4,6,41]).

In conclusion, the general model presented here contains two simplifying assumptions that, while reasonable, may not be justified under all circumstances.

(1) It is assumed that fiber growth takes place only via addition of monomer at fiber ends. A more general model would allow for fiber growth by addition of soluble oligomers (e.g. dimers, trimers, etc.) as well as monomers to the growing fiber. It should be pointed out that the very long period of time that is calculated for the distribution

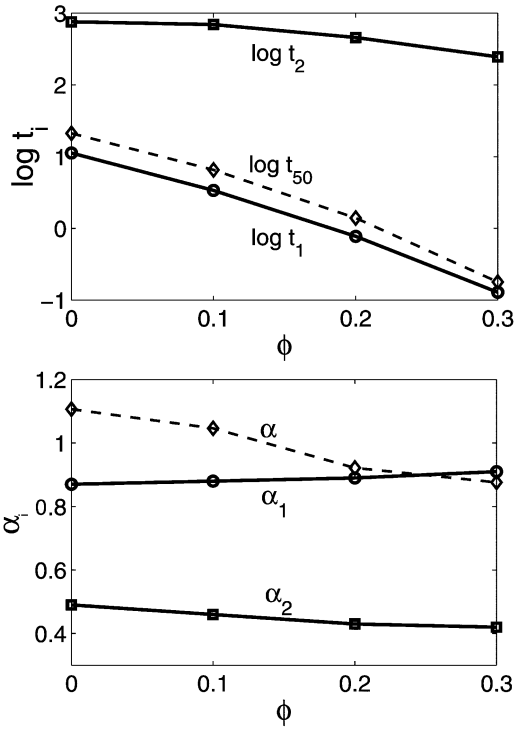

Fig. 12. ϕ-Dependence of best-fit values of $\log t_1$, $\log t_2$, α_1 and α_2 obtained from fitting Eq. (27) to $g_{poly}(t^*)$ (Fig. 10B), and ϕ-dependence of $\log t_{50}$ and α calculated for f_{poly} (t^*) (Fig. 10A).

of fiber lengths to reach equilibrium is a direct consequence of the assumption that fibers may change length only via association and dissociation of monomer from fiber ends. If the length of fibers may be altered via additional mechanisms such as association and dissociation of oligomers, or breakage and annealing of fibers [42–44], one would expect the equilibrium distribution of polymer lengths to be more rapidly attained.

(2) It is assumed that nucleation is exclusively homogeneous. The kinetics of formation of fibers of deoxygenated sickle Hb in highly nonideal solution have been well described by a model specifying both homogeneous and heterogeneous nucleation [26], but the extent to which heterogeneous nucleation is a general feature of protein fiber formation is unknown. It is of interest to note that the initial motivation for the incorporation of heterogeneous nucleation into the sickle Hb polymerization model was the observation of significant kinetic cooperativity, which could not be accounted for by early models of fiber formation incorporating only homogeneous nucleation. The model presented here, on the other hand, can in some limiting kinetic regimens (see left hand panel of Fig. 7) account for kinetic cooperativity without invoking heterogeneous nucleation.

Acknowledgments

D. Hall would like to acknowledge the United States government and the Human Frontiers Society for financial assistance in the form of a Fogarty Visiting Fellowship and a Human Frontiers Long Term Fellowship (which, respectively, financed the initial and end components of his contribution to this work).

References

[1] F. Oosawa, M. Kasai, Theory of linear and helical aggregations of macromolecules, J. Mol. Biol. 4 (1962) 10–21.
[2] F. Oosawa, S. Asakura, Thermodynamics of the Polymerization of Protein, Academic Press, New York, 1975.
[3] T.L. Hill, Linear Aggregation Theory in Cell Biology, Springer, New York, 1987.
[4] F. Gaskin, C.R. Cantor, M.L. Shelanski, Turbidimetric studies of the in vitro assembly and disassembly of porcine neurotubules, J. Mol. Biol. 89 (1974) 737–755.
[5] L.S. Tobacman, E.D. Korn, The kinetics of actin nucleation and polymerization, J. Biol. Chem. 258 (1983) 3207–3214.
[6] W.A. Eaton, J. Hofrichter, Sickle cell hemoglobin polymerization, Adv. Protein Chem. 40 (1990) 63–279.
[7] C. Frieden, D.W. Goddette, Polymerization of actin and actin-like systems: evaluation of the time course of polymerization in relation to the mechanism, Biochemistry 22 (1983) 5836–5843.
[8] C. Frieden, Actin and tubulin polymerization: the use of kinetic models to determine mechanism, Annu. Rev. Biophys. Biophys. Chem. 14 (1985) 189–210.
[9] R.F. Goldstein, L. Stryer, Cooperative polymerization reactions. Analytical approximations, numerical examples, and experimental strategy, Biophys. J. 50 (1986) 583–599.
[10] A. Wegner, J. Engel, Kinetics of the cooperative association of actin to actin filaments, Biophys. Chem. 3 (1975) 215–225.
[11] H. Flyvbjerg, E. Jobs, S Leibler, Kinetics of self-assembling microtubules: an 'inverse problem' in biochemistry, Proc. Natl. Acad. Sci. USA 93 (1996) 5975–5979.
[12] F. Ferrone, Analysis of protein aggregation kinetics, Meth. Enzymol. 309 (1999) 256–274.
[13] A.P. Minton, Excluded volume as a determinant of macromolecular structure and reactivity, Biopolymers 20 (1981) 2093–2120.
[14] L.W. Nichol, A.G. Ogston, P.R. Wills, Effect of inert polymers on protein self-association, FEBS Lett. 126 (1981) 18–20.
[15] A.P. Minton, The effect of volume occupancy upon the thermodynamic activity of proteins: some biochemical consequences, Mol. Cell. Biochem. 55 (1983) 119–140.
[16] S.B. Zimmerman, A.P. Minton, Macromolecular crowding: biochemical, biophysical, and physiological consequences, Annu. Rev. Biophys. Biomol. Struct. 22 (1993) 27–65.
[17] A.P. Minton, Implications of macromolecular crowding for protein assembly, Curr. Opinion Struct. Biol. 10 (2000) 34–39.
[18] P.D. Ross, A.P. Minton, The effect of non-aggregating proteins upon the gelation of sickle cell hemoglobin: model calculations and data analysis, Biochem. Biophys. Res. Commun. 88 (1977) 1308–1314.
[19] R.L. Tellam, M.J. Sculley, L.W. Nichol, P.R. Wills, The influence of poly(ethylene glycol) 6000 on the properties of skeletal-muscle actin, Biochem. J. 213 (1983) 651–659.
[20] J. Wilf, J.A. Gladner, A.P. Minton, Acceleration of fibrin gel formation by unrelated proteins, Thromb. Res. 37 (1985) 681–688.
[21] N. Cole, G.B. Ralston, Enhancement of self-association of human spectrin by polyethylene glycol, Int. J. Biochem. 26 (1994) 799–804.

[22] R. Lindner, G. Ralston, Effects of dextran on the self-association of human spectrin, Biophys. Chem. 57 (1995) 15–25.
[23] R.A. Lindner, G.B. Ralston, Macromolecular crowding: effects on actin polymerization, Biophys. Chem. 66 (1997) 57–66.
[24] G.J. Rivas, J.A. Fernandez, A.P. Minton, Direct observation of the enhancement of noncooperative protein self- assembly by macromolecular crowding: indefinite linear self-association of bacterial cell division protein FtsZ, Proc. Natl. Acad. Sci. USA 98 (2001) 3150–3155.
[25] M.F. Bishop, F.A. Ferrone, Kinetics of nucleation-controlled polymerization. A perturbation treatment for use with a secondary pathway, Biophys. J. 46 (1984) 631–644.
[26] F.A. Ferrone, J. Hofrichter, W.A. Eaton, Kinetics of sickle hemoglobin polymerization. II. A double nucleation mechanism, J. Mol. Biol. 183 (1985) 611–631.
[27] D. Hall, A.P. Minton, Effects of inert volume-excluding macromolecules on protein fiber formation. I. Equilibrium models, Biophys. Chem. 98 (2002) 93–104.
[28] A. Minton, Effects of excluded surface area and adsorbate clustering on surface adsorption of proteins. II. Kinetic models, Biophys. J. 80 (2001) 1641–1648.
[29] A.G. Ogston, The spaces in a uniform random suspension of fibres, Trans. Faraday Soc. 54 (1958) 1754–1757.
[30] J.L. Lebowitz, E. Helfand, E. Praestgaard, Scaled particle theory of fluid mixtures, J. Chem. Phys. 43 (1965) 774–779.
[31] J.C. Giddings, E. Kucera, C.P. Russell, M.N. Myers, Statistical theory for the equilibrium distribution of rigid molecules in inert porous networks. Exclusion chromatography, J. Phys. Chem. 72 (1968) 4397–4408.
[32] A.G. Ogston, On the interaction of solute molecules with porous networks, J. Phys. Chem. 74 (1970) 668–669.
[33] M.A. Cotter, Hard spherocylinders in an anisotropic mean field, J. Chem. Phys. 66 (1977) 1098–1106.
[34] W.H. Press, S.A. Teukolsky, W.T. Vetterling, B.P. Flannery, Numerical Recipes: the Art of Scientific Computing, Cambridge University Press, Cambridge [Cambridgeshire], New York, 1986.
[35] C.W. Gear, The automatic integration of ordinary differential equations, Commun. ACM 14 (1974) 176–179.
[36] F. Oosawa, Size distribution of protein polymers, J. Theory Biol. 27 (1970) 69–86.
[37] R.M. Gibbons, The scaled particle theory for mixtures of hard convex particles, Mol. Phys. 18 (1970) 809–816.
[38] D. Hall, A.P. Minton, Macromolecular Crowding: qualitative and semi-quantitative, quantitative challenges, Biochim. Biophys. Acta 1649 (2003) 127–139.
[39] L. Edelstein-Keshet, G.B. Ermentrout, Models for the length distributions of actin filaments: I. Simple polymerization and fragmentation, Bull. Math. Biol. 60 (1998) 449–475.
[40] G.B. Ermentrout, L. Edelstein-Keshet, Models for the length distributions of actin filaments: II. Polymerization and fragmentation by gelsolin acting together, Bull. Math. Biol. 60 (1998) 477–503.
[41] J.J. Correia, R.C. Williams Jr., Mechanisms of assembly and disassembly of microtubules, Annu. Rev. Biophys. Bioeng. 12 (1983) 211–235.
[42] M. Kawamura, K. Maruyama, Electron microscopic particle length of F-actin polymerized in vitro, J. Biochem. (Tokyo) 67 (1970) 437–457.
[43] M. Kawamura, K. Maruyama, A further study of electron microscopic particle length of F-actin polymerized in vitro, J. Biochem. (Tokyo) 72 (1972) 179–188.
[44] E. Andrianantoandro, L. Blanchoin, D. Sept, J.A. McCammon, T.D. Pollard, Kinetic mechanism of end-to-end annealing of actin filaments, J. Mol. Biol. 312 (2001) 721–730.